An Independent, Temperature-Controllable Microelectrode Array

ARTICLE *in* ANALYTICAL CHEMISTRY · APRIL 2004

Impact Factor: 5.64 · DOI: 10.1021/ac035270p · Source: PubMed

5 AUTHORS, INCLUDING:

Haesik Yang
Pusan National University
114 PUBLICATIONS **2,445** CITATIONS
SEE PROFILE

Chang Auck Choi
Electronics and Telecommunications Resear…
62 PUBLICATIONS **409** CITATIONS
SEE PROFILE

Kwang Hyo Chung
Electronics and Telecommunications Resear…
44 PUBLICATIONS **412** CITATIONS
SEE PROFILE

Chi-Hoon Jun
Electronics and Telecommunications Resear…
51 PUBLICATIONS **259** CITATIONS
SEE PROFILE

Anal. Chem. **2004,** *76,* 1537−1543

An Independent, Temperature-Controllable Microelectrode Array

Haesik Yang,* Chang Auck Choi, Kwang Hyo Chung, Chi-Hoon Jun, and Youn Tae Kim

BioMEMS Group and Microsystem Group, Electronics and Telecommunications Research Institute (ETRI), Daejeon 305-350, Korea

Rapid, localized temperature control and negligible power consumption are key requisites for realizing effective parallel and sequential processing in the miniaturized, integrated biomedical microdevices where temperature-dependent biochemical reactions and fluid flow occur. In this study, an independent, temperature-controllable microelectrode array, with excellent temperature control rates and minimal power consumption, has been developed using microelectromechanical systems technology. The microfabricated array consists of Pt microelectrodes (100-μm diameter), with n-doped polysilicon microheaters (1.4-kΩ resistance), and vacuum-sealed cavities of depth 6.2 μm and diameter 200 μm. The thermal characteristics of each microelectrode were evaluated electrochemically through surface temperature measurements. The large heater power coefficient (2.1 $\pm$ 0.1 °C mW^{-1}) and the short heating and cooling times (less than 0.2 s for $T_{0.95}$) are consequences of the vacuum-sealed cavities, which facilitate good thermal isolation and low thermal mass. The temperature of each microelectrode is independently controlled by a dedicated microheater, without thermally influencing the adjacent microelectrodes significantly.

Miniaturized and integrated biomedical microdevices have played a crucial role in the advance of molecular diagnostics, genomics, and proteomics.[1−4] However, the exact control of biochemical reactions and fluid flow is difficult to accomplish in devices of this size. The methods employed to implement such control sometimes involve temperature modulation because these methods require no mechanical operations, making them highly advantageous for miniaturization.[5] Thermal methods have been applied to a variety of microdevice applications, including the micropatterning or binding of biomolecules,[5−8] cell culture,[9] microreactors,[10,11] microfluidics,[12−18] and biochemical reaction on surface.[19] These methods operate through thermally induced changes in either thermopneumatic volume,[16] surface hydrophobicity/hydrophilicity,[5,7,9] surface tension,[13] viscosity,[14,15] and intermolecular interactions[19] or through the thermally induced swelling/deswelling of hydrogels.[12,18]

Site-selective temperature control is a prerequisite for both parallel and sequential processing of arrayed biomolecules,[20] multiple biochemical reactions,[21,22] and complex fluid flows.[13,15] Moreover, the rapid and precise regulation of temperature is necessary for fast and accurate analysis. Thus, it is important to develop microdevices in which these parameters are met, while a minimal amount of power is consumed. For example, a thermal gradient DNA chip has been devised that controls site-selective DNA hybridization.[19] On the other hand, a patterned microelectrode array has been utilized for the immobilization of biomolecules,[5,23] for electrochemical detection,[24] and for electrowetting control.[25,26] Providing the individual microelectrodes are thermally isolated, their respective surface temperatures can be indepen-

* To whom correspondence should be addressed. E-mail: hsyang@etri.re.kr. Tel.: 82-42-860-6876. Fax: 82-42-860-6836.

(1) Sanders, G. H. W.; Manz, A. *Trends Anal. Chem.* **2000**, *19*, 364−378.
(2) Dario, P.; Carrozza, M. C.; Benvenuto, A.; Menciassi, A. *J. Micromech. Microeng.* **2000**, *10*, 235−244.
(3) Huan, Y.; Mather, E. L.; Bell, J. L.; Madou, M. *Anal. Bioanal. Chem.* **2002**, *372*, 49−65.
(4) Tüdos, A. J.; Besselink, A. J.; Schasfoort, B. M. *Lab Chip* **2001**, *1*, 83−95.
(5) Huber, D. L.; Manginell, R. P.; Samara, M. A.; Kim, B.-I.; Bunker, B. C. *Science* **2003**, *301*, 352−354.
(6) Ding, Z.; Fong, R. B.; Long, C. J.; Stayton, P. S.; Hoffman, A. S. *Nature* **2001**, *411*, 59−62.
(7) Nath, N.; Chilkoti, A. *Anal. Chem.* **2003**, *75*, 709−715.
(8) Malmstadt, N.; Yager, P.; Hoffmann, A. S.; Stayton, P. S. *Anal. Chem.* **2003**, *75*, 2943−2949.
(9) Yamato, M.; Konno, C.; Utsumi, M.; Kikuchi, A.; Okano, T. *Biomaterials* **2002**, *23*, 561−567.
(10) Slyadnev, M. N.; Tanaka, Y.; Tokeshi, M.; Kitamori, T. *Anal. Chem.* **2001**, *73*, 4037−4044.
(11) Kopp, M. U.; de Mello, A. J.; Manz, A. *Science* **1998**, *280*, 1046−1048.
(12) Yu, C.; Mutlu, S.; Selvaganapathy, P.; Mastrangelo, C. H.; Svec, F.; Fréchet, J. M. J. *Anal. Chem.* **2003**, *75*, 1958−1961.
(13) Sammarco, T. S.; Burns, M. A. *AIChE J.* **1999**, *45*, 350−366.
(14) Buchholz, B. A.; Doherty, E. A. S.; Albarghouthi, M. N.; Bogdan, F. M.; Zahn, J. M.; Barron, A. E. *Anal. Chem.* **2001**, *73*, 157−164.
(15) Liu, Y.; Rauch, C. B.; Stevens, R. L.; Lenigk, R.; Yang, J.; Rhine, D. B.; Grodzinski, P. *Anal. Chem.* **2002**, *74*, 3063−3070.
(16) Selvaganapathy, P.; Carlen, E. T.; Mastrangelo, C. H. *Sens. Actuators, A* **2003**, *104*, 275−282.
(17) Sethu, P.; Mastrangelo, C. H. *Sens. Actuators, A* **2003**, *104*, 283−289.
(18) Harmon, M. E.; Tang, M.; Frank, C. W. *Polymer* **2003**, *44*, 4547−4556.
(19) Kajiyama, T.; Miyahara, Y.; Kricka, L. J.; Wilding, P.; Graves, D. J.; Surrey, S.; Fortina, P. *Genome Res.* **2003**, *13*, 467−475.
(20) Okano, K.; Yasuda, K.; Ishiwata, S. *Sens. Actuators, B* **2000**, *64*, 88−94.
(21) Zou, Q.; Miao, Y.; Chen, Y.; Sridhar, U.; Chong, C. S.; Chai, T.; Tie, Y.; The, C. H. L.; Lim, T. M.; Heng, C. *Sens. Actuators, A* **2002**, *102*, 114−121.
(22) Kuwata, M.; Sudo, H.; Kawano, K.; Miyazaki, K. *Micro Total Anal. Syst.* **2002**, *2*, 715−717.
(23) Heller, M. J.; Forster, A. H.; Tu, E. *Electrophoresis* **2000**, *21*, 157−164.
(24) Umek, R. M.; Lin, S. W.; Vielmetter, J.; Terbrueggen, R. H.; Irvine, B.; Yu, C. J.; Kayyem, J. F.; Yowanto, H.; Blackburn, G. F.; Farkas, D. H.; Chen, Y.-P. *J. Mol. Diagn.* **2001**, *3*, 74−84.
(25) Yoon, J.-Y.; Garrell, R. L. *Anal. Chem.* **2003**, *75*, 5097−5102.
(26) Paik, P.; Pamula, V. K.; Pollack, M. G.; Fair, R. B. *Lab Chip* **2003**, *3*, 28−33.

10.1021/ac035270p CCC: $27.50
Published on Web 02/03/2004

dently regulated to generate precise, independent control over biochemical reactions or electrochemical reactions. Accordingly, an independent, temperature-controllable microelectrode array, in which the surface temperature is both controlled and rapid, is essential for the parallel and sequential processing of biomedical microdevices.

To date, temperature-controllable electrodes have found wide application in electrochemistry,[27−33] and as such, many electrode heating methods have been developed for this purpose. The heating methods developed initially typically relied on radiation sources such as pulsed lasers,[34] tungsten lamps,[35] and radio frequency-induced methods;[36] however, precise temperature adjustments were difficult to achieve with these methods. The direct Joule heating method (Gründler et al..),[27,28,31] in which an electrode is heated by a high-frequency alternating current, also has a problem that alternating current influences the redox current. These methods consume considerable amounts of electrical power and are difficult to incorporate in miniaturized devices.

Microelectromechanical systems (MEMS) technology is frequently used in the fabrication of miniaturized devices.[37] MEMS-based microdevices such as PCR microchips[11,38,39] and gas microsensors[40] typically utilize microheaters to induce localized heating. If a microelectrode is located near a microheater, then part of the heat generated through Joule heating is invariably transferred to the electrode itself. MEMS-based microdevices are usually constructed from silicon, a substance that exhibits a large thermal conductivity. When the Si device contains a heating element, then it is necessary to minimize the power lost through the Si substrate by thermally isolating the microheater, maximizing heat transfer to the microelectrode. Thermal isolation is implemented by either etching a pit around the microheater or introducing a cavity between the Si substrate and the microheater.[37] These procedures reduce the thermal mass considerably, leading to rapid temperature regulation. The formation of etched pits or cavities is achieved through bulk or surface micromachining technology.[37] Bulk micromachining[41] essentially involves etching of the upper[42] or lower surfaces of the Si substrate, while surface micromachining[43] etches only thin films that have been deposited on the Si. The microdevices proposed here, will invariably be exposed to biological fluids which demand that the etched pits or cavities be isolated from solution.

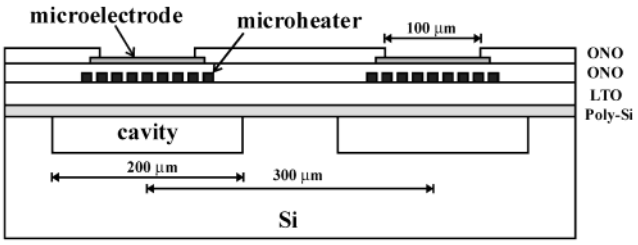

Figure 1. Schematic side view of an independent, temperature-controllable microelectrode array.

In this study, we outline steps to prepare an independent, temperature-controllable microelectrode array, in which each unit cell comprises a microheater, a deep vacuum-sealed cavity for good thermal isolation and low thermal mass, and a microelectrode to effect the desired electrochemical reaction or biomolecule immobilization (Figure 1). The electrical isolation between the microheater and microelectrode, the passivation of interconnects and microelectrodes, and the small resistance associated with the interconnects are all taken into consideration in the design of the microfabrication process. Furthermore, the thermal characteristics of the array, including the heating power efficiency, the heating and cooling rates, and the independent temperature control, are all investigated through indirect measurements of the microelectrode surface temperature.

EXPERIMENTAL SECTIONS

Chemicals, Electrochemistry, and Simulation. Potassium ferricyanide ($K_3[Fe(CN)_6]$), potassium ferrocyanide ($K_4[Fe(CN)_6]$), and potassium nitrate (KNO_3) were all purchased from Aldrich and used as received. Doubly distilled water was used in the preparation of all solutions.

All electrochemical experiments were performed using a CHI model 660A potentiostat/galvanostat (CH Instruments, Austin, TX) interfaced with a PC and a three-electrode cell consisting of a microfabricated microelectrode, a Ag/AgCl (3 M NaCl) reference electrode, and a platinum wire counter electrode. All potentials were reported relative to the Ag/AgCl reference electrode. The cell temperature was maintained at 20.0 °C by circulating thermostated water through a cell jacket. The microelectrode array (excluding the pads) was dipped in a KNO_3-containing solution to determine its thermal characteristics. The chip has large pads that have 1-mm pitch and 3-mm length, and the pads are connected to external power supply and potentiostat. Square wave voltages were applied to the microheater using an HP 3325B function generator (Agilent).

CFD-ACE+, an advanced multiphysics solver, was used to perform numerical simulations of the temperature of electrode. Detailed information is shown in the Supporting Information.

Device Microfabrication. An illustration of the general microfabrication process, combined with side views of a single unit cell, is shown in Figure 2. The device was fabricated from p-type ⟨100⟩ 5-in. Si wafers, and eight photomasks were used

(27) Gründler, P. *Fresenius J. Anal. Chem.* **1998**, *362*, 180−183.
(28) Gründler, P.; Kirbs, A. *Electroanalysis* **1999**, *11*, 223−228.
(29) Voss, T.; Kirbs, A.; Gründler, P. *Fresenius J. Anal. Chem.* **2000**, *367*, 320−323.
(30) Wang, J.; Gründler, P.; Flechsig, G.-U.; Jasinski, M.; Rivas, G.; Sahlin, E.; Paz, J. L. L. *Anal. Chem.* **2000**, *72*, 3752−3756.
(31) Baranski, A. S. *Anal. Chem.* **2002**, *74*, 1294−1301.
(32) Voss, T.; Gründler, P.; Brett, C. M. A.; Brett, A. M. O. *J. Pharm. Biomed. Anal.* **1999**, *19*, 127−133.
(33) Flechsig, G.-U.; Korbout, O.; Hocevar, S. B.; Thongngamdee, S.; Ogorevc, B.; Gründler, P.; Wang, J. *Electroanalysis* **2002**, *14*, 192−196.
(34) Smalley, J. F.; Geng, L.; Feldberg, S. W. *J. Electroanal. Chem.* **1993**, *356*, 181−200.
(35) Rotenberg, Z. A. *J. Electroanal. Chem.* **1993**, *345*, 469−474.
(36) Qiu, F.; Comption, R. G.; Coles, B. A.; Marken, F. *J. Electroanal. Chem.* **2000**, *492*, 150−155.
(37) Baltes, H.; Paul, O.; Brand, O. *Proc. IEEE* **1998**, *86*, 1660−1678.
(38) Woolley, A. T.; Hadley, D.; Landre, P.; deMello, A. J.; Mathies, R. A.; Northrup, M. A. *Anal. Chem.* **1996**, *68*, 4081−4086.
(39) Krika, L. J.; Wilding, P. *Anal. Bioanal. Chem.* **2003**, *377*, 820−825.
(40) Simon, I.; Bârsan, N.; Bauer, M.; Weimar, U. *Sens. Actuators, B* **2001**, *73*, 1−26.
(41) Kovacs, G. T. A.; Maluf, N. I.; Petersen, K. E. *Proc. IEEE* **1998**, *86*, 1536−1551.
(42) Klaassen, E. H.; Reay, R. J.; Strorment, C.; Kovacs, G. T. A. *Sens. Actuators, A* **1997**, *58*, 43−50.
(43) Bustillo, J. M.; Howe, R. T.; Muller, R. S. *Proc. IEEE* **1998**, *86*, 1552−1574.

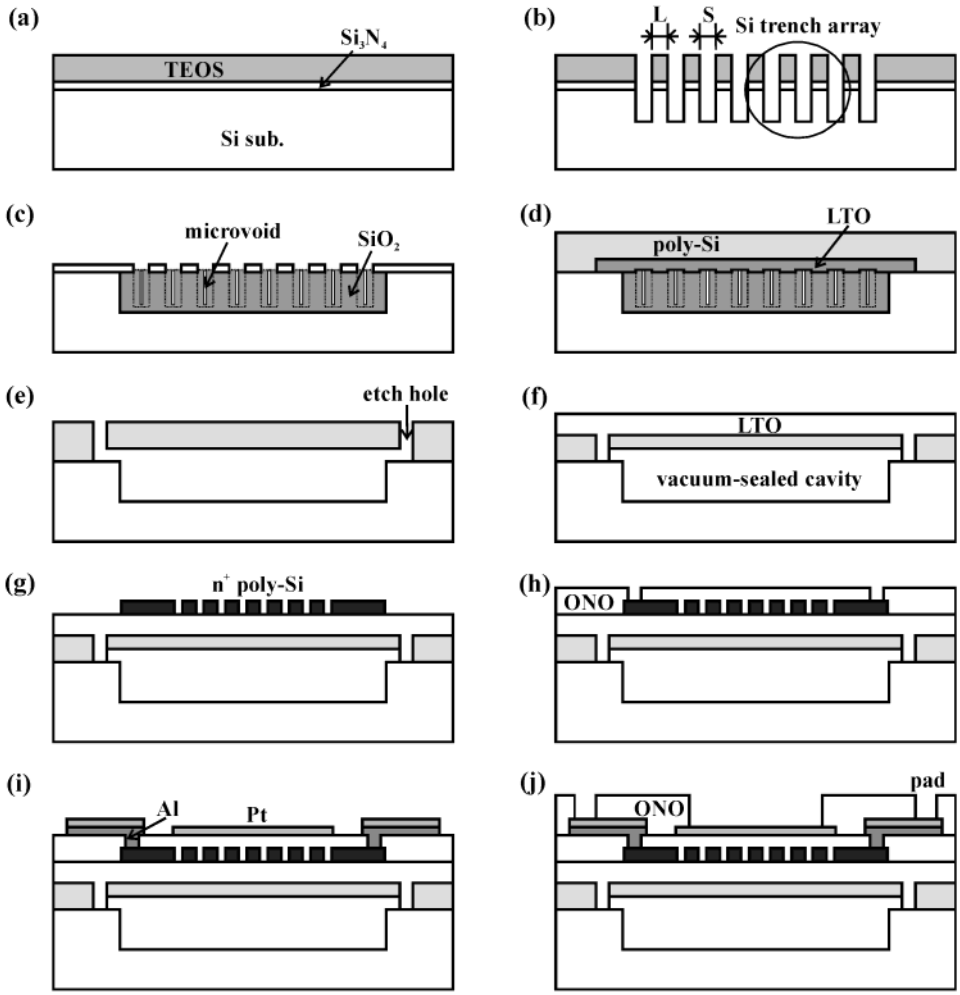

Figure 2. Microfabrication process sequence for an independent, temperature-controllable microelectrode array.

during entire process. The fabrication process can be divided into two parts. In the first part, deep, vacuum-sealed cavities and multilayered membranes were formed on Si substrates (Figure 2a−f),[44] whereas the shallow vacuum-sealed cavity was reported previously by Liu and Tai.[45] Essentially, trenchlike (Si) arrays are formed in Si substrates. These features, which were subsequently transformed to sacrificial silicon oxide layers by thermal oxidation, were wet-etched in a concentrated hydrofluoric acid solution to form deep cavities. In the second part, a microheater was fabricated on the membrane, and then the microelectrode, interconnects, and pads were formed (Figure 2g−j).

After a standard cleaning procedure, low-pressure chemical vapor deposition (LPCVD) silicon nitride (Si_3N_4; 1200 Å, 800 °C, 290 mTorr, $N_2/SiH_2Cl_2/NH_3$ = 500 sccm/200 sccm/500 sccm) and LPCVD tetraethyl orthosilicate (TEOS) SiO_2 (8000 Å, 720 °C, 350 mTorr, N_2/TEOS = 1000 sccm/200 sccm) films were deposited on the cleaned Si wafers (Figure 2a). A photoresist layer was deposited on top of the substrate and then exposed through a photomask to produce a trenchlike array, with a line and space (L/S) ratio of 0.45 (0.8 μm): >0.55 (Figure 2b). The Si_3N_4 layer acts as a masking layer to prevent thermal oxidation of the Si surface during subsequent thermal oxidation (Figure 2c), while the SiO_2 layer acts as a masking layer to prevent Si_3N_4 etching during the subsequent Si dry etching step (Figure 2b). After development of the photoresist, the exposed SiO_2 and Si_3N_4 regions were then etched by reactive ion etching (RIE). The remaining photoresist was removed, and the exposed Si was then etched by RIE to form an array of Si trenches with depth of ≥5 μm (Figure 2b).

The Si trenches were n-doped with phosphorus oxychloride ($POCl_3$) at 900 °C for 30 min, to improve both the Si oxidation rate (during subsequent thermal oxidation) and the thermal oxide etching rate. After removal of the remaining (TEOS) SiO_2 layer by wet etching in a 6:1 buffered hydrofluoric acid (BHF) solution, the array was then oxidized at 1000 °C for 5 h in a pyrogenic environment (Figure 2c). The defined cavity region was subsequently filled with thick thermal oxide and microvoid columns. The microvoids act as microcapillary channels, which enhance etchant penetration into the cavity region during the subsequent thermal oxide etching process. The remaining Si_3N_4 film was removed by soaking in a phosphoric acid solution, and a low-temperature silicon oxide (LTO) film (4500 Å) was then deposited on the substrate by LPCVD (400 °C, 240 mTorr, SiH_4/O_2 = 100 sccm/400 sccm). A photoresist was deposited on the LTO film and then exposed through a second mask. The exposed LTO was

(44) Jun, C.-H.; Choi, C.-A.; Jang, W.-I.; Kim Y. T. *Proc. SPIE−Int. Soc. Opt. Eng.* **2000**, *4174*, 164−171.
(45) Liu, C.; Tai, Y.-C. *IEEE J. Microelectromech. Syst.* **1999**, *8*, 135−145.

etched in a 6:1 BHF solution, and the remaining photoresist removed (Figure 2d). The patterned LTO layer acts as an etchant passage to the thermal oxide cavity region, passing through the polysilicon (poly-Si) etch hole formed in the subsequent step. A poly-Si layer (1.6 μm), which behaves as a mechanically supporting layer during subsequent HF etching, was deposited by LPCVD (625 °C, 200 mTorr, $N_2/SiH_4 = 500$ sccm/200 sccm). This layer was then postannealed at 1000 °C for 2 h to relieve the compressive stress associated with poly-Si (Figure 2d).

A photoresist layer was deposited on the poly-Si film and exposed through a third mask to produce a pattern of four holes, which were subsequently etched into the poly-Si by RIE. After removal of the remaining photoresist, the removal of the sacrificial thermal oxide and LTO layers by wet etching in a concentrated HF solution for 2 h (Figure 2e) yielded the desired cavity, which was vacuum-dried at 450 °C to remove residual moisture. The poly-Si membrane was thinned to 0.35 μm by a poly-Si RIE process. Finally, a second LTO layer (1.6 μm) was then deposited on the poly-Si membrane under reduced pressure (240 mTorr) to form a protective coating over the etched holes (Figure 2f). As a result, a deep vacuum-sealed cavity is formed in which the LTO layer acts as not only a sealing layer but also an insulating layer between the poly-Si and microheater.

In standard CMOS processes, there are essentially two materials used to fabricate microheaters, doped poly-Si and platinum. Here, n-doped poly-Si was elected on the basis that the adhesion layer for Pt such as titanium exhibits a high diffusion rate at high temperatures, which gives a bad effect on Pt. First, a poly-Si layer (4000 Å) was deposited on the stacked LTO/poly-Si membrane by LPCVD. This was then followed by $POCl_3$ doping at 900 °C for 30 min to reduce film resistance. A photoresist layer was deposited on the n-doped poly-Si film and then patterned through a fourth mask to define the microheater pattern. The exposed n-doped poly-Si was then etched by RIE and the remaining photoresist removed (Figure 2g).

The current generated by a microheater can influence the redox current associated with the corresponding microelectrode. It is therefore important to reduce this cross-talk, as even small leakage currents between the microelectrode and microheater will significantly impact the low-level redox currents in the microelectrode. To improve the electrical isolation between the microheater and microelectrode, subsequent layers of LTO (3000 Å), LPCVD Si_3N_4 (3000 Å), and LTO (3000 Å) were deposited on the microheater. A photoresist layer was deposited on the LTO film and then patterned with a fifth mask to define the contact holes. The exposed LTO/LPCVD Si_3N_4/LTO (LPCVD ONO) layer was then etched by RIE and the remaining photoresist removed (Figure 2h).

Aluminum is often used as an interconnect material in standard CMOS processes; however, its poor corrosion resistance makes it difficult to utilize in microfabricated microelectrodes. Pt on the other hand, shows good corrosion resistance; however, its resistivity is much larger than that of Al. The temperature-controllable microelectrode array reported here requires several interconnects, particularly between the microheaters and pads. Moreover, the combined resistance of the two interconnects must be significantly smaller than that of the actual microheater. Consequently, Al was adopted as the interconnect material, except in the areas around the microelectrodes, to exclude the possibility of Al corrosion. To ensure the contact between n-doped poly-Si and Al, a Pt layer was deposited (300 Å) by sputtering and then sintered at 460 °C under N_2/H_2 for 15 min. The remaining Pt was removed with a 1:3 solution of H_2SO_4/HCl at 60 °C, and then titanium tungsten (2200 Å) and Al (8000 Å) layers were sputtered sequentially on the substrate surface. A photoresist layer was then deposited on the TiW/Al film and patterned through a sixth mask to define the interconnects and pads. The exposed TiW/Al was then etched by RIE and the remaining photoresist removed. Additional TiW (2200 Å) and Pt (2000 Å) layers were then deposited sequentially by sputtering. A further photoresist layer deposited on the TiW/Pt film was patterned with a seventh mask to define the electrode area. The exposed TiW/Pt was then etched by ICP etcher (600 Å/min, 10 mTorr, $Ar/Cl_2 = 70$ sccm/30 sccm) and the photoresist removed (Figure 2i).

The use of Al interconnects in microfabricated devices invariably requires a good passivation layer to prevent corrosion. It was reported that the plasma-enhanced chemical vapor deposition (PECVD) ONO structure shows excellent passivation properties.[46] Consequently, the sequential deposition of PECVD SiO_2 (1300 Å, 400 °C), PECVD Si_3N_4 (5400 Å, 400 °C), and PECVD SiO_2 (1300 Å, 400 °C), provides an effective ONO passivation layer to prevent unwanted Al corrosion. A photoresist layer was deposited on the PECVD ONO structure and then patterned with a final eighth mask to define the electrode open area. The exposed ONO layer was subsequently etched by RIE and the residual photoresist removed (Figure 2j), to obtain an independent, temperature-controlled microelectrode array.

RESULTS AND DISCUSSION

SEM micrographs of the independent, temperature-controllable microelectrode array (plane views) are shown in Figure 3. Figure 3a shows a closeup image of a single unit cell, which houses a microelectrode (100-μm diameter), a spiral microheater (1.4-kΩ resistance), and a multilayered membrane (200-μm diameter) positioned above the vacuum-sealed cavity, and four etch holes. Figure 3b shows an array consisting of four microelectrodes, where the adjacent microelectrodes and adjacent membranes are 200 and 100 μm apart, respectively. Each microelectrode is individually addressable in terms of current and potential control. SEM micrographs of the unit cell (cross-sectional views) are shown in Figure 4, where the depth of the microfabricated cavity ($\sim$6.2 μm) has been determined from the image in Figure 4c. The micrograph shows that the deep cavity is formed well, though some SiO_2 residues remain in the cavity. Moreover, the protective membrane formed over the cavity appears quite smooth, where no signs of cracking or peeling were observed during the subsequent processes following cavity formation.

To investigate the thermal characteristics of the microfabricated device, measurement of the temperature of the electrode surface during both heating and cooling of the microheater is required. For temperature measurement, it is usual in microfabricated devices to use thin-film temperature sensors such as resistive temperature detector, thermistor, and thermocouple.[49]

(46) Schmitt, G.; Schultze, J.-W.; Fassbender; F.; Buss, G.; Lüth, H.; Schöning, M. J. *Electrochim. Acta* **1999**, *44*, 3865−3883.
(47) Opallo, M. *J. Electroanal. Chem.* **1998**, *446*, 39−45.
(48) Zerihun, T.; Gründler, P. *J. Electroanal. Chem.* **1996**, *404*, 243−248.

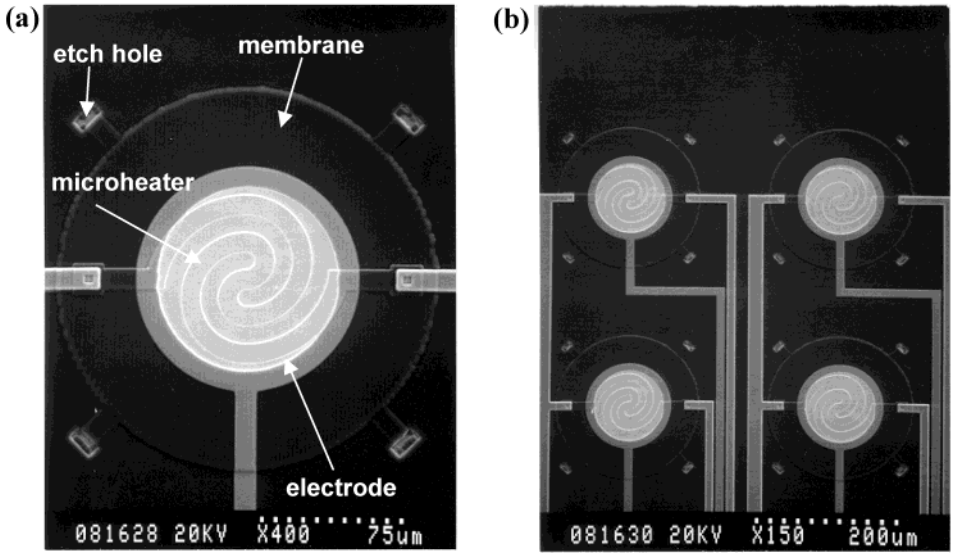

Figure 3. SEM micrographs of (a) a microfabricated temperature-controllable microelectrode and (b) an independent, temperature-controllable microelectrode array (plane views).

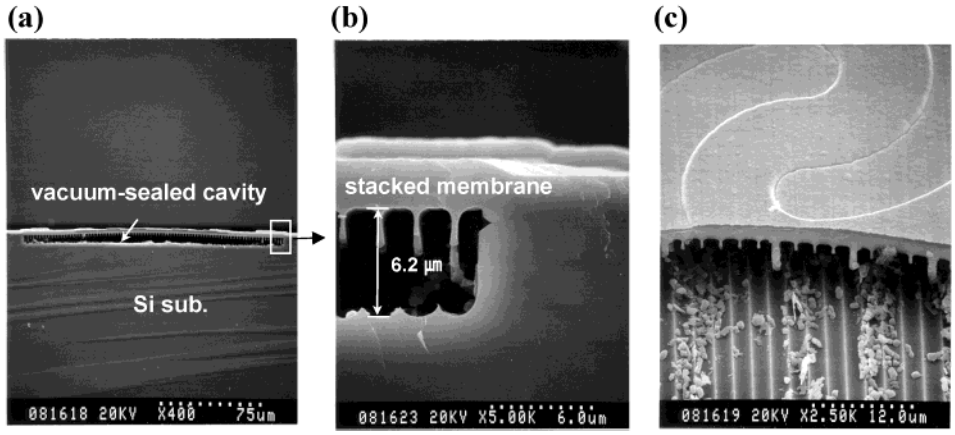

Figure 4. (a) SEM micrographs of (a) a microfabricated temperature-controllable microelectrode, (b) a partially magnified view of (a) (cross-sectional views), and (c) a cracked membrane (slant view).

However, the number of interconnects accompanied by the temperature sensors increases as the number of arrays increases. Moreover, additional fabrication processes are required to make the sensors. The redox potential of a couple on the other hand, is linearly dependent on the temperature and can be measured by monitoring the open circuit potential (OCP) of an electrode in solutions containing the redox couple. Consequently, the temperature of the electrode surface can be measured by monitoring OCP. The temperature dependence of the ferricyanide/ferrocyanide couple redox potential is typically larger than those of other redox couples,[47] making it suitable for the measurement of the microelectrode surface temperature.

The distance between the microheater and the corresponding microelectrode is typically 9000 Å. When dc voltage is applied to the microheater, a large nonfaradaic decaying current is induced in the microelectrode, providing invalid OCP information, which invariably leads to inaccurate temperature readings. To minimize this problem, square-wave voltages with a frequency of 1 kHz and amplitude equivalent to the applied voltage are applied to the microheater. The dependence of OCP on the applied voltage in a solution containing 5 mM $K_3Fe(CN)_6$, 5 mM $K_4Fe(CN)_6$, and 0.5 M KNO_3 is demonstrated in Figure 5a. As the applied voltage is increased, the OCP decreases and eventually returns to its original value after cycling through a series of voltage steps. This indicates that the changes in the thermal performance of the microheater are insignificant during both the heating and cooling processes. Considering that the temperature coefficient of the redox potential is 1.56 mV $°C^{-1}$,[48] the dependence of the electrode temperature on the microheater power can be obtained (as shown in Figure 5b), where at 7 V, the average temperature of the Pt surface is ~95 °C.

In general, the temperature of a heater is proportional to its heating power. Consequently, for the microelectrode array described here, the electrodes are located in proximity to the corresponding microheaters, such that their surface temperature is roughly proportional to the power of the microheater (Figure 5b). The coefficient of the electrode temperature on the heating power of the microheater can be defined, because the line is essentially linear. The calculated coefficient is 2.1 ± 0.1 °C mW^{-1}, whereas the coefficient obtained from an approximated simulation is 2.0 °C mW^{-1}. The large value implies that a significant amount

(49) Jiang, L.; Wong, M.; Zohar, Y. *Measure. Sci. Technol.* **1999**, *8*, 653−664.

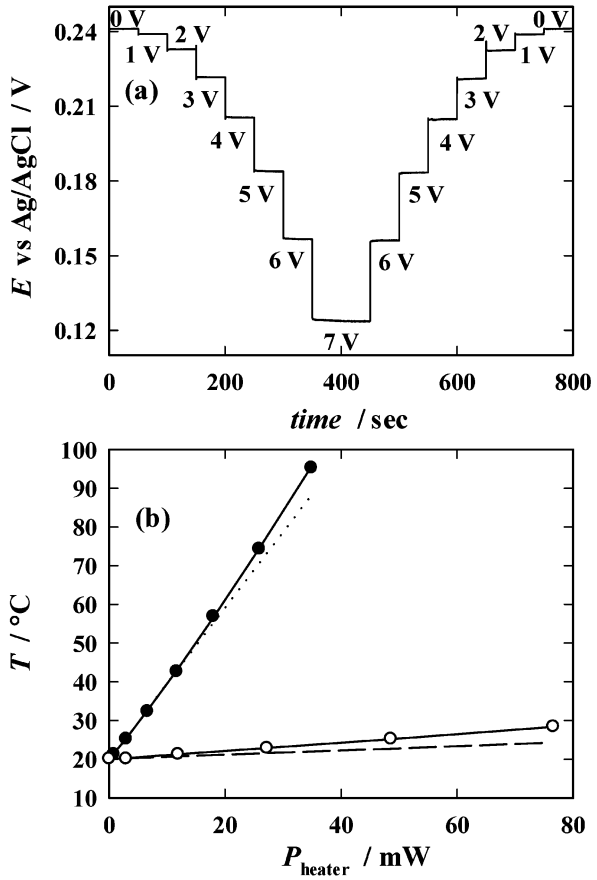

Figure 5. (a) Dependence of the open circuit potential on the applied voltage of a microheater in a solution containing 5 mM $K_3Fe(CN)_6$, 5 mM $K_4Fe(CN)_6$, and 0.5 M KNO_3 and (b) dependence of the electrode temperature on the power of a microheater (closed circle, experimental value for a cavity-containing device; dotted line, simulated value for a cavity-containing device; open circle, experimental value for a cavity-less device; dashed line, simulated value for a cavity-less device).

of heat generated by the microheater is transferred to the microelectrode. The coefficient for a cell containing no cavity was also measured, to determine the effect of the vacuum-sealed cavity on thermal isolation (Figure 5b). At an applied potential of 10 V, the temperature of the Pt surface changed by just ~8 °C, where the coefficient for this system was calculated as 0.11 °C mW^{-1}, and the simulated value determined as 0.06 °C mW^{-1}. The experimentally determined value is typically 19 times smaller than that of the cavity-containing device, due to the large thermal conductivity of Si. The amount of heat that dissipates from the microheater into the cavity-less Si substrate is quite considerable, compared to the system with the deep vacuum-sealed cavity. Thus, it is clearly evident that the deep cavity beneath the microheater, coupled with the inclusion of vacuum sealing, plays a significant role in the thermal isolation of the system. The heating power of the microheater is limited due to its chemical composition, which alters as the power is increased. In the absence of a cavity, the power consumption expended in the heating process is particularly large. In this experiment, however, it is impossible to heat the microelectrode above 40 °C without affecting the thermal performance of the microheater. On the other hand, no thermal performance changes are observed during cyclic heating and cooling in the cavity-containing device between 20 and 95 °C.

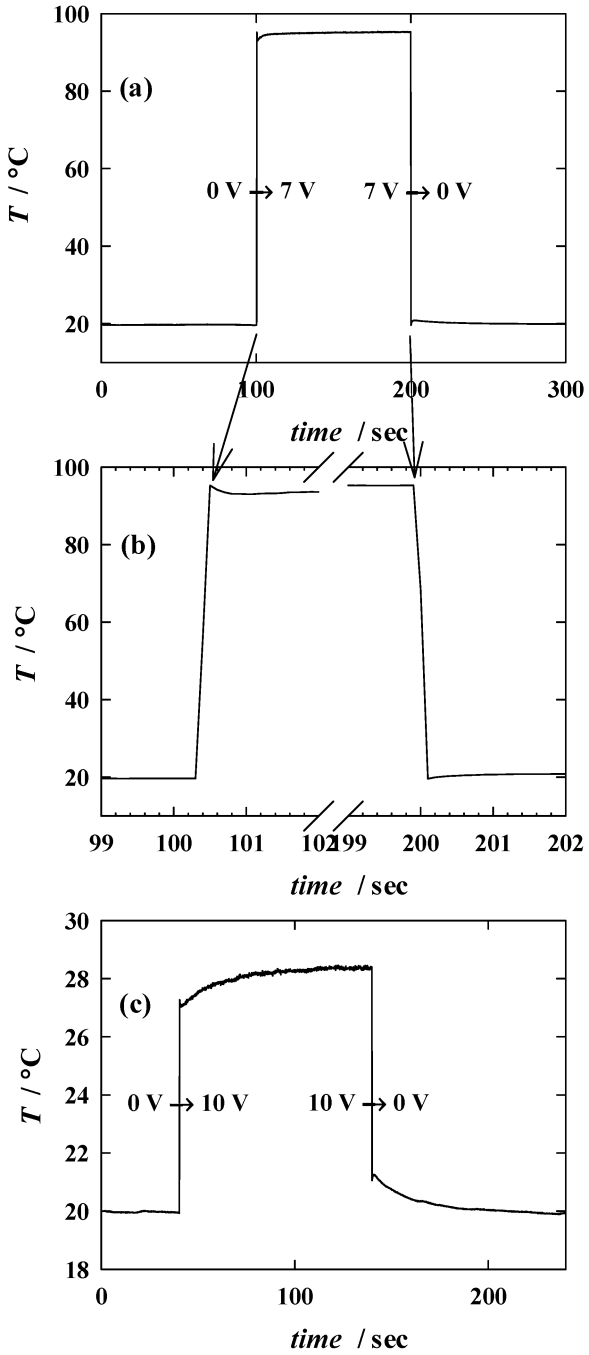

Figure 6. (a) Temperature changes during heating and cooling when a cavity exists, (b) a partially magnified view of (a), and (c) temperature changes when a cavity does not exist.

Consequently, the presence of a cavity is necessary for heating microelectrodes to high temperatures as well as for thermal isolation.

Rapid temperature control and low power consumption are important factors that need to be addressed in the design of microfabricated heating devices. To determine the rates of heating and cooling, it is necessary to measure the temperature changes during large voltage steps (as shown in Figure 6a), a magnified view of which is shown in Figure 6b. The temperature reaches 95% of the steady state value within 0.2 s during both heating (0−7 V) and cooling (7−0 V) (Figure 6b). It is interesting to note that both the heating and cooling processes are particularly rapid,

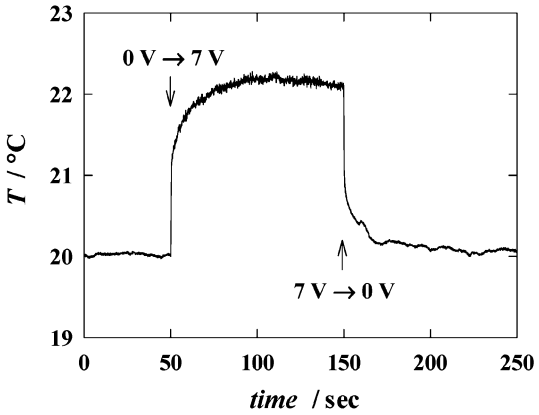

Figure 7. Temperature changes of a microelectrode when an adjacent microelectrode is heated from 20 to 95 °C and then cooled from 95 to 20 °C.

despite the considerable time taken to heat or cool the solution near the microelectrode. The heating and cooling rates in the cavity-less heating device take approximately 10 and 6 s, respectively, to arrive at 95% of the steady-state value (Figure 6c). Both values are much larger than those obtained for the cavity-containing device, clearly indicating that the large Si thermal mass around the microheater requires longer heating and cooling times. Hence, the use of a vacuum-sealed cavity enables both rapid heating and cooling.

For parallel temperature control, the temperature of each microelectrode within the array must be controlled independently. However, there is a possibility that heat generated by the microheaters might also influence the temperature of adjacent microelectrodes. To address this issue, a microelectrode was heated from 20 to ~95 °C (0−7 V), while the temperature of the adjacent microelectrode was monitored (Figure 7). As the temperature was increased (~75 °C), the temperature of the adjacent electrode changed by only ~2 °C before steady state was achieved. This small temperature difference demonstrates that the heat from the microheater has little effect on the adjacent microelectrode, despite the short distance (200 μm) between the two electrodes, suggesting that each unit cell is thermally isolated. Generally, the temperature perturbation is much smaller than 75 °C in the biomedical microdevices, except for the PCR chip. Thus, small temperature perturbation would give negligible effect on the adjacent microelectrode. Probably, the Si that exists between the two membranes reduces the amount of heat transferred to the adjacent electrode. The small temperature change observed in adjacent electrodes suggests that the temperature of each electrode can be controlled almost independently.

CONCLUSIONS

We have developed a microarray composed of microelectrodes with independently adjustable temperature control, as implemented by dedicated microheaters. The fabrication of a deep, vacuum-sealed cavity beneath the microheater gives rise to increased thermal isolation and reduced thermal mass, leading to reduced power consumption and improved heating and cooling rates, respectively.

With further enhancements to the microfabricated structure, the reality of an array comprising independent, temperature-controlled microelectrodes that could regulate biochemical reactions such as DNA hybridization rapidly and independently is a distinct possibility. Moreover, by reducing the size of the unit cell (microheater and microelectrode) still further, a significant increase in array density, combined with reduced power consumption, could be realized.

ACKNOWLEDGMENT

This work has been supported in part by the Ministry of Information and Communication of Korea and in part by the Ministry of Science and Technology of Korea through the NRL program.

SUPPORTING INFORMATION AVAILABLE

Details of numerical simulations on the temperature of microelectrode. This material is available free of charge via the Internet at http://pubs.acs.org.

Received for review October 28, 2003. Accepted January 2, 2004.

AC035270P